Coastal Dynamics 2017
Paper No. 188

INCLUSION OF WAVE BREAKING TURBULENCE IN REFERENCE CONCENTRATION MODELS

Joep van der Zanden[1], Àngels Fernàndez-Mora[1], Dominic van der A[2], David Hurther[3], Iván Cáceres[4], Tom O'Donoghue[2] and Jan Ribberink[1]

Abstract

Most commonly applied models for reference concentrations or sediment pickup rates do not account for wave breaking effects on sand resuspension. Consequently, they tend to underpredict the suspended sand load in the surf zone. Here, we present a new method to account for wave breaking turbulence effects in reference concentration models or pickup functions. An adapted reference concentration model is validated using recent laboratory measurements of near-bed turbulent kinetic energy and suspended sand concentration, yielding good agreement ($r^2 = 0.60$).

Key words: sediment transport, wave breaking, suspended sediment, wave flume experiment, turbulence, morphodynamic models.

1. Introduction

Morphodynamic models typically use an advection-diffusion model to calculate the transport of suspended sediment. Depth-resolving advection-diffusion models rely on semi-empirical formulations to quantify the vertical sediment exchange between the bed load and the suspension layers. Such formulations prescribe either a concentration at an elevation close to the bed (i.e. reference concentration approach) or an upward sand flux (i.e. pickup function approach) (Nielsen, 1992). For non-breaking waves, such functions generally use the bed shear stress by waves and currents as driving force for sand suspension (e.g. Nielsen, 1986; Van Rijn, 1984a, 1984c, 2007; Zyserman & Fredsøe, 1994).

However, such formulations have limited predictive capability when applied to the wave breaking region (Aagaard & Jensen, 2013), because breaking waves – especially strongly plunging waves – may directly entrain large amounts of sand from the bed (Nielsen, 1984). Several studies have shown that suspension events under breaking waves follow directly after the intermittent arrival of breaking-generated turbulent vortices (Nadaoka *et al.*, 1988; Scott *et al.*, 2009; Yoon & Cox, 2012). This turbulent suspension can be physically explained by high instantaneous bed shear stresses (Cox & Kobayashi, 2000; Zhou *et al.*, 2017) and by upward-directed pressure gradients in the sand bed (Sumer *et al.*, 2013) under breaking-generated turbulent vortices. Especially under plunging-type breaking waves, near-bed breaking-generated turbulent kinetic energy (TKE) can show clear phase variation (Ting & Kirby, 1995), which may contribute to phase-dependent sand suspension and to net wave-related suspended sediment transport (Yoon & Cox, 2012; Brinkkemper *et al.*, 2017; Van der Zanden *et al.*, 2017).

Based on such observations of enhanced sand suspension in the wave breaking region, several parameterisations have been proposed to include wave breaking effects on sand pickup rate and reference concentration models. Some studies related the reference concentration to the near-bed TKE, either directly (Steetzel, 1993) or indirectly as an additional parameter to increase the bed shear stress and sand suspension (Hsu & Liu, 2004; Okayasu *et al.*, 2010). These formulations are consistent with the aforementioned observed relationship between sand suspension and wave breaking turbulence arrival at the bed. Other studies relate the reference concentration to the local (breaking) wave conditions, using parameters such as the wave height at breaking (Jayaratne & Shibayama, 2007), the local wave height and water depth (Mocke & Smith, 1992), and the wave or roller energy dissipation (Kobayashi & Johnson, 2001; Smith & Mocke, 1993; Spielmann *et al.*, 2004). The advantage of such models is that they are more robust and do not rely on detailed numerical predictions of wave breaking generated turbulence dynamics. However, this is at the same time a drawback, since wave breaking TKE spreads vertically and

[1]Water Engineering and Management department, University of Twente, Netherlands. J.vanderZanden@utwente.nl, M.FernandezMora@utwente.nl, J.S.Ribberink@utwente.nl.
[2] School of Engineering, University of Aberdeen, UK. D.A.vanderA@abdn.ac.uk, T.ODonoghue@abdn.ac.uk
[3] LEGI-CNRS, University of Grenoble, France. David.Hurther@legi.cnrs.fr
[4] CIEMLAB, Universitat Politècnica de Catalunya, Spain. I.Caceres@upc.edu

horizontally through advection and diffusion processes, leading to an increase in near-bed TKE and sand pickup not only in the region of intense wave breaking but also at adjacent shoaling and inner surf zone locations (e.g. van der Zanden *et al.*, 2016, 2017).

None of the aforementioned parameterisations that account for wave breaking effects on sand pickup has been widely incorporated in common morphodynamic models. This is possibly because most of these formulations are highly empirical, yet were calibrated/validated for a limited number of observations of surf zone suspended sand concentrations – none of which provided measurements of concurrent near-bed TKE and sand concentration.

In the present paper, we present a new parameterization to account for wave breaking turbulence effects on sediment resuspension in reference concentration or pickup models. The parameterization is theoretically derived on the basis of existing, widely applied formulations for pickup and for near-bed TKE (Section 2). Subsequently, in Section 3, the new formulation is validated using recent laboratory measurements of near-bed TKE and suspended sand concentrations under a large-scale plunging breaking wave (Van der Zanden *et al.*, 2016, 2017). Section 4 discusses the outcomes and the applicability of the new model.

2. Derivation of adapted reference concentration model for breaking waves

This section presents a method for including wave breaking turbulence effects in suspended sand pick-up and reference concentration models. The method is developed on the basis of theoretical considerations, using Van Rijn's (1984c) reference concentration model as a framework. Note that effects of external (wave breaking) turbulence are accounted for by adapting the bed shear stress formulation, and the presented approach could easily be applied to other reference concentration or pickup models.

2.1. *Van Rijn's (1984c) C_0 model for shear flows without external turbulence*

Van Rijn (1984b, 1984c) defines a bedload and a suspended load layer that are vertically separated at a reference elevation (z_a) with respect to the local bed level. For plane bed (sheet flow) conditions, z_a = 0.01 m, while it is equal to half the bedform height when bedforms are present. The reference elevation is typically inside the wave bottom boundary layer. The net vertical sand flux $\phi_z(z_a)$ between the bedload and the suspension layer is the result of an upward diffusive flux and a downward flux due to sand settling (Van Rijn, 1984c):

$$\phi_z(z_a) = -\frac{\nu + \nu_t}{\sigma_c}\frac{\partial C(z_a)}{\partial z} - w_s C(z_a) \tag{1}$$

here σ_c is the Schmidt number, w_s is the sand settling velocity, and ν and ν_t are the kinematic molecular and turbulent diffusivity, respectively. The upward diffusive flux is physically explained by the turbulent diffusion of sand particles in the direction of the lowest concentration. In the following, this vertical flux is termed the pickup rate (annotated ϕ_p), i.e.:

$$\phi_p = -\frac{\nu + \nu_t}{\sigma_c}\frac{\partial C(z_a)}{\partial z} \tag{2}$$

For turbulent flows, $\nu_t >> \nu$, hence it follows that ϕ_p is driven by vertical turbulent velocity fluctuations w' and that ϕ_p can be assumed proportional to the near-bed vertical turbulence intensity w'_{rms} (Van Rijn, 1984c). In a crucial next step, Van Rijn (1984c) relates w'_{rms} to the bed shear velocity u_* by assuming that the turbulence that drives ϕ_p is entirely generated locally by bed friction. For steady uniform wall flows without additional external turbulence, experimental observations and numerical simulations have indeed shown that w'_{rms} in the log region relates to u_* as (e.g. Pope, 2000):

$$w'_{rms} \approx u_* \tag{3}$$

Note that this is also consistent with experimental observations of $u'_{rms}/u_* = 1.7$ by Sumer *et al.* (2003) for mobile sand beds, given that the ratio of vertical to horizontal turbulence intensity $w'_{rms}/u'_{rms} \approx 0.6$ for the log law layer in steady flows (Pope, 2000). Following similar argumentation, Van Rijn (1984c), replaced w'_{rms} by u_* as the driving force in his model formulations. The major advantage is that u_* is a more pragmatic and more widely applied variable than w'_{rms} for use in sand transport models.

Van Rijn (1984c) proposes that a sand particle can be picked up when u_* exceeds the particle's critical shear velocity for sand suspension, $u_{*,cr}$, i.e.:

$$\phi_p = 0 \qquad \text{if } u_* \le u_{*,cr} \tag{4}$$

The pick-up rate ϕ_p is proportional to the dimensionless transport parameter T_ϕ which expresses the difference between the exerted and critical bed shear stress:

$$T_\phi = \frac{u_*^2 - u_{*,cr}^2}{u_{*,cr}^2} \qquad \text{for } u_* > u_{*,cr} \tag{5}$$

Based on experimental observations, Van Rijn finally proposed the following equation for the instantaneous sand pick-up rate (Van Rijn, 1984a)

$$\phi_p = 3.3 \cdot 10^{-4} T_\phi^{1.5} D_*^{0.3} \qquad \text{for } u_* > u_{*,cr} \tag{6}$$

and for the instantaneous volumetric reference concentration C_0 (Van Rijn, 1984c)

$$C_0 = 0.015 \frac{D_{50}}{z_a} \frac{T_\phi^{1.5}}{D_*^{0.3}} \qquad \text{for } u_* > u_{*,cr} \tag{7}$$

where D_{50} is the median sand diameter; and D_* is the dimensionless particle diameter:

$$D_* = D_{50} \left[\frac{(s-1)g}{\nu^2} \right]^{1/3} \tag{8}$$

Here, $s = 2.65$ is the relative density of sand grains in water; and g is the gravitational acceleration. The critical bed shear velocity by Van Rijn (1984c) is given by

$$u_{*,cr} = \frac{4 w_s}{D_*} \tag{9}$$

2.2. *The inclusion of external turbulence*

When external turbulence invades the boundary layer, the assumption that near-bed turbulence is entirely produced by local bed friction and that w'_{rms} can be equated to u_* (Eq. 3) becomes invalid. Therefore, the transport parameter T_ϕ (Eq. 5) should be reformulated to account for the effects of external turbulence on sand suspension. Note that u_* was introduced in Eq. (5) as substitution for the vertical turbulence intensity w'_{rms}. The latter, in return, is proportional to the local turbulent kinetic energy k_* that is entirely due to local production by bed friction:

$$u_*^2 = {w'_{rms}}^2 = \alpha k_* \tag{10}$$

The value for α varies greatly with distance from the bed. For the present purpose, it makes sense to choose an α value corresponding with the reference elevation z_a, which for most waves at field-scale would correspond to the logarithmic region of the wave boundary layer. Proposed values for $\alpha = {w'_{rms}}^2 / k_*$ are in the range of 0.2 (Svendsen, 1987, inner layer of WBL) to 0.3 (Pope, 2000, log region steady flow boundary layer). One may also deduce the value of α from the common boundary condition for bed shear produced turbulence, which reads (Hinze, 1975; used for oscillatory WBLs by e.g. Kranenburg *et al.*, 2012; Ruessink *et al.*, 2009):

$$k_* = u_*^2 / \sqrt{C_\mu} \tag{11}$$

where the constant $C_\mu = 0.09$. Combining equations (10) and (11) yields $\alpha = \sqrt{C_\mu} = 0.3$, which is consistent with experimental observations (Pope, 2000). Substitution of Eq. (11) into Eq. (5) then yields:

$$T_\phi = \frac{\sqrt{C_\mu} k_* - u_{*,cr}^2}{u_{*,cr}^2} \qquad \text{for } \sqrt{C_\mu} k_* > u_{*,cr}^2 \tag{12}$$

Equations (12) and (5) are equivalent for boundary layer flows where only bed friction affects the near-bed turbulent kinetic energy. For flows with an additional turbulence source, the total near-bed TKE (k_b) is the sum of locally produced bed shear TKE (k_*) and external TKE which is in the present study produced by wave breaking (k_{wbr}):

$$k_b = k_* + k_{wbr} \tag{13}$$

For flows with an additional source of turbulence we now assume that sand suspension still scales to the near-bed TKE:

$$T_\phi = \frac{\sqrt{C_\mu}k_b - u_{*,cr}^2}{u_{*,cr}^2} \qquad \text{for } k_b > \frac{u_{*,cr}^2}{\sqrt{C_\mu}} \tag{14}$$

Equation (14) provides an adapted transport parameter that uses k_b instead of u_* as governing variable for pickup rate or reference concentration. Eq. (14) can be directly applied in combination with Eq. (6), (7) and (8) to predict sand pick-up rates or reference concentration for situations with and without wave breaking turbulence. Note that in the absence of an external turbulence source, $k_b = k_*$ and Eq. (14) returns to the original formulation by Van Rijn (1984c) – provided that Eq. (11) is used as boundary condition for TKE at the bed.

Eq. (14) can also be interpreted in terms of an adapted bed shear velocity $u_{*,kb}$ by the combined orbital flow and external turbulence, i.e.

$$T_\phi = \frac{u_{*,kb}^2 - u_{*,cr}^2}{u_{*,cr}^2} \qquad \text{for } u_{*,kb}^2 > u_{*,cr}^2 \tag{15}$$

$$u_{*,kb} = C_\mu^{1/4}\sqrt{k_b} \tag{16}$$

In measurements, it will often be impossible to separate the "bed shear" and "external" contributions to k_b. However, in some numerical models, both TKE sources can be separated. Rewriting the latter equation gives

$$u_{*,kb} = C_\mu^{1/4}\sqrt{k_* + k_{wbr}} \tag{17}$$

Substitution of (11) in (17) yields the following expression for the adapted bed shear velocity:

$$u_{*,kb}^2 = u_*^2 + \sqrt{C_\mu}k_{wbr} \tag{18}$$

Here, the second term represents the additional apparent bed shear for sand pickup due to external turbulence. Finally, the latter equation can also be rewritten in terms of the free-stream orbital plus wave-related velocity u as:

$$u_{*,kb}^2 = 0.5f_{wc}u_0^2 + \sqrt{C_\mu}k_{wbr} = 0.5f_{wc}\left(u_0^2 + \frac{0.6}{f_{wc}}k_{wbr}\right) \tag{19}$$

where f_{wc} is the combined wave plus current friction factor and u_0 is the free-stream velocity due to waves and currents. If follows that the relative significance of k_{wbr} with respect to u_0^2 for sand pickup depends on the factor $0.6/f_{wc}$. For flows with high f_{wc} (e.g. rough beds, bed forms), bed shear will lead to more local turbulence production and sand resuspension, hence the relative importance of k_{wbr} for sand pickup will be lower.

3. Experimental validation

The model is validated using high-resolution near-bed measurements of turbulent kinetic energy and suspended sand concentrations under plunging breaking waves obtained during a recent large-scale laboratory experiment (Van der Zanden *et al.*, 2016; 2017 – vdZ16 and vdZ17 in what follows). The experiment shed new insights into wave breaking effects on wave bottom boundary layer velocity and turbulence (vdZ16), on the spatio-temporal variation of suspended sand concentration and fluxes (vdZ17), and on sheet flow dynamics, grain sorting, and sand bar morphodynamics (Van der Zanden, 2016; Van der Zanden *et al.*, Submitted). The reader is referred to these papers for more detailed descriptions of the experiment and its results; a brief summary is presented in this section.

3.1 Description of experiments

The experimental set-up is shown in Figure 1. The initial bed profile consisted of an offshore 1:10 slope, followed by a breaker bar-trough configuration, an elongated gradually sloping inner surf zone, and a parabolic dissipative beach. The test section consisted of a mobile sand bed (well-sorted medium sand, D_{50} = 0.25 mm, measured w_s = 0.034 m/s) between x = 35 to 68 m; the beach profile at x > 68 m was fixed with geotextile. The experiment involved regular waves with wave height H = 0.85 m and wave period T = 4 s at water depth h = 2.55 m near the wave paddle. One experimental repeat consisted of six 15-minute runs during which the mobile bed profile developed. After this 90-minute experiment the flume was drained and the initial bed profile was restored. This experimental procedure was repeated 12 times. Figure 1 indicates definitions of cross-shore coordinate x and vertical coordinates z and ζ, where the latter is the elevation with respect to the local bed level (i.e. $\zeta = z - z_{bed}$).

A mobile frame, custom-built for this project (Ribberink *et al.*, 2014), was used to deploy the primary measurement instrumentation: an acoustic concentration and velocity profiler (ACVP) (Hurther *et al.*, 2011), three acoustic Doppler velocimeters (ADVs), a six-nozzle transverse suction system (TSS), and a pressure transducer (PT). For each experimental repeat the mobile frame was positioned to a different cross-shore location. This

procedure with 12 experimental repeats resulted in a high spatial coverage of measurements (Figure 1b). Two CCM$^+$ tanks (Van der Zanden *et al.*, 2015) were installed slightly offshore from the bar crest to measure sheet flow concentration and particle velocity. The water surface elevation was measured by sidewall-deployed resistive wave gauges (RWGs) and PTs. Finally, the bed profile was measured before each experiment and after every second run using echo sounders. The experiment and data processing steps of all instruments are described in more detail in vdZ16 and vdZ17.

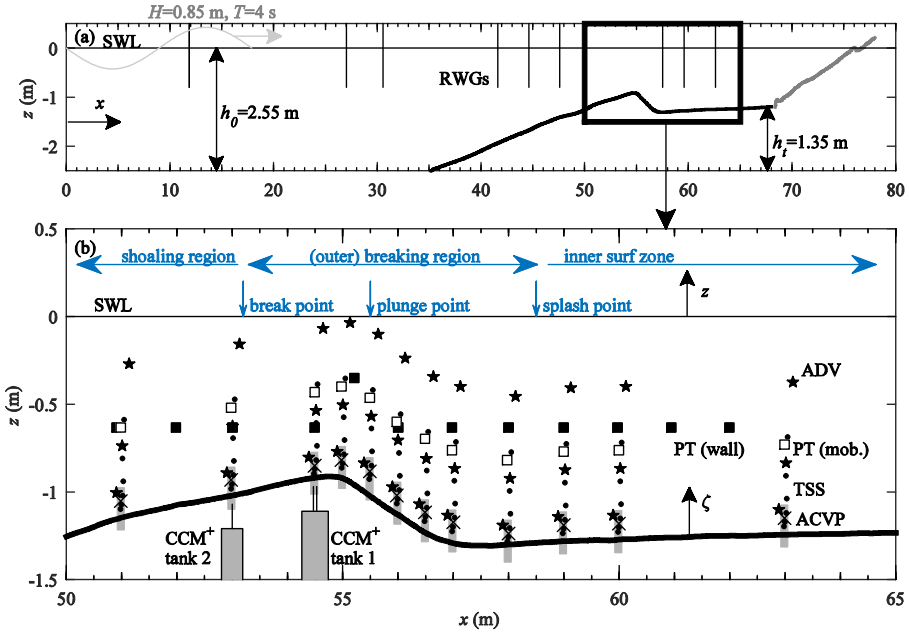

Figure 1. Experimental set-up: (a) bed profile (solid line) and locations of resistive wave gauges (vertical lines); (b) measurement locations of ADVs (star symbols), Transverse Suction System nozzles (black dots), pressure transducers (squares), ACVP (grey rectangles), and two CCM$^+$ tanks.

The waves breaking over the bar crest were characterized as plunging breakers. Figure 1b indicates characteristic locations of the breaking process, i.e. the 'break point' where the wave starts to overturn (x = 53.0 m); the 'plunge point' where the breaking jet hits the water surface (x = 55.5 m); and the 'splash point' where the wave has transformed into a surf bore (x = 58.5 m). This characterises the shoaling region, breaking region and inner surf zone (Figure 1b) following the terminology by Svendsen *et al.* (1978).

3.2 Measured hydrodynamics and suspended sand concentration

Figure 2a shows the maximum and minimum phase-averaged water surface level η. The wave height decreases by approximately 50% between the break point and the splash point. The time-averaged water surface level follows a net set-down before breaking that transforms into net set-up in the inner surf zone (x > 58.5 m).

Figure 2b shows the time-averaged and the maximum and minimum phase-averaged near-bed horizontal velocity. The orbital velocity amplitude decreases strongly between the breaker bar and trough (from x = 55.0 to 57.0 m) due to the decrease in wave energy and the increase in water depth. Over the same region, the offshore-directed undertow increases in magnitude, with particularly strong currents (exceeding –0.5 m/s at ζ = 0.10 m) observed around x = 57.0 m. The velocity is strongly non-uniform in this region (high $|d\bar{u}/dx|$). It follows from fluid mass conservation that the gradients in $d\bar{u}/dx$ are balanced by time-averaged velocities in the vertical direction, directed upward above the bar crest (for x = 55.5 – 57.0 m where $d\bar{u}/dx < 0$) and downward above the bar trough (for x = 57.0 – 59.0 m where $d\bar{u}/dx > 0$). This time-averaged fluid circulation was confirmed by measurements from an accompanying fixed-bed experiment involving the same wave condition and bed profile (Van der A *et al.*, 2017).

Figure 2c shows the time-averaged turbulent kinetic energy (TKE) at free-stream elevation and inside the wave bottom boundary layer (WBL). TKE increases by an order of magnitude in the breaking region (x = 53.0 – 58.0 m) relative to the shoaling zone (x = 51.0 m). This increase in TKE occurs regardless of the reduction in $\langle u \rangle_{max}$ and $\langle u \rangle_{min}$ magnitudes, which indicates that wave breaking is the main source for the TKE increase. The increase in TKE occurs both at free-stream and WBL elevations, suggesting that breaking-generated turbulence even invades the WBL.

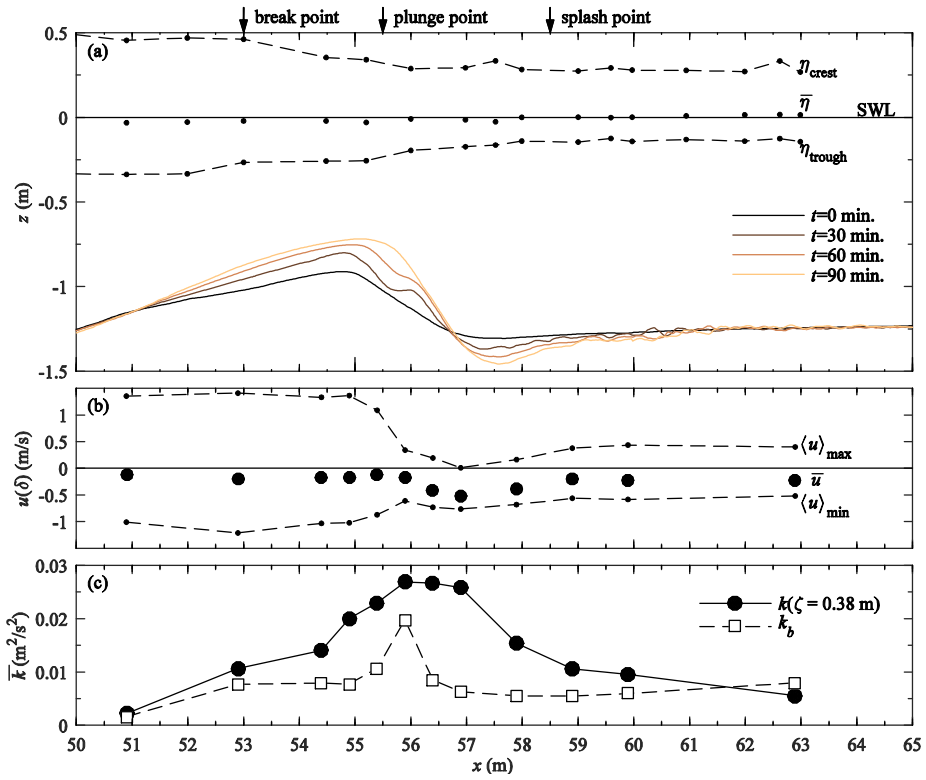

Figure 2. (a) Maximum, minimum and mean phase-averaged water surface level (dots and dashed lines) over the evolving bed profile (solid lines); (b) Maximum, minimum (dots and dashed line) and mean phase-averaged horizontal velocity u (circles) at the WBL overshoot elevation δ ($\zeta \approx 0.01$ m); (c) Time-averaged TKE at free-stream elevation $\zeta = z - z_{bed} = 0.38$ m (circles) and maximum time-averaged TKE inside the WBL (squares). The hydrodynamic measurements are taken during the first 15 minutes of the experiment ($t = 0 - 15$ min.).

Figure 3 shows the suspended sediment concentration measured with TSS (circles). The profiles can be described with a power function (e.g. Kobayashi *et al.*, 2005):

$$C(\zeta) = C_0(\zeta/z_a)^{-1/m} \tag{20}$$

Here, C_0 is the reference concentration at reference elevation $\zeta = z_a$ and m is a vertical mixing parameter. The solid curves and background color contour in Figure 3 show the inter- and extrapolated time-averaged concentration obtained by fitting Eq. (20) through the TSS measurements.

Suspended sand concentrations vary by orders of magnitude in both the horizontal and vertical directions. In the wave breaking region concentrations are up to two orders of magnitude higher than in the shoaling zone and inner surf zone. Highest concentrations are measured close to the bed between the bar crest and bar trough (x = 55.0 to 57.0 m), i.e. in close vicinity of the plunge point at x = 55.5 m.

The vertical mixing parameter m and reference concentration C_0 are explored in more detail through Figure 4. Figure 4a reveals strong vertical mixing (high m) of suspended sediment above the bar crest (x = 53.0 to 55.0 m). Two mechanisms are considered mainly responsible for this strong mixing: (i) advection by upward time-averaged velocities resulting from the two-dimensional undertow circulation; (ii) vertical diffusion by breaking-generated turbulence. High values of m around x = 58.0 m imply that suspended sand is also well-mixed above the bar trough. However, due to the non-uniform flow conditions, sand concentrations are not purely controlled by local (vertical) advection and diffusion. Gradients of horizontal sand flux indicate that at the bar trough, a significant influx of sand occurs high in the water column, which may explain the near depth-uniform concentration profiles in this region (vdZ17).

Figure 4b shows the reference concentration C_0, which increases strongly (by an order of magnitude) from the shoaling to the breaking region, with a local maximum of around 30 kg/m^3 at (x = 56.0 m), i.e. 0.5 m shoreward from the plunge point. Further shoreward, C_0 rapidly decreases between x = 56.0 and 57.0 m. Low C_0 values maintain in the bar trough (x = 57.0 – 58.0 m), and C_0 remains approximately constant throughout the inner surf zone (x = 59.0 – 63.0 m). By comparing Figure 4b and Figure 2b, it follows that the cross-shore distribution of C_0 varies notably from the distribution of maximum onshore and offshore velocity. These cross-shore distributions,

and poor correlation coefficients following linear regression between $\bar{u}$ and C_0 and between $\tilde{u}_{rms}$ and C_0 (vdZ17), indicate that the orbital and time-averaged velocity is a poor predictor for sand resuspension in the present experiment. The cross-shore distribution of C_0 (Figure 4b) is instead similar to distributions of the near-bed turbulent kinetic energy k_b (Figure 2c). Indeed, linear regression between both variables revealed significant correlation with r^2 = 0.51 (vdZ17). This result is consistent with previous observations of (intermittent) resuspension following breaking-generated eddy arrival at the bed (Nadaoka et al., 1988; Nielsen, 1984; Scott et al., 2009), which has been physically explained by high instantaneous turbulent bed shear stresses (Cox *et al.*, 1996; Zhou et al., 2017) and by upward-directed pressure gradients in the bed that occur directly under large-scale vortices (Sumer et al., 2013).

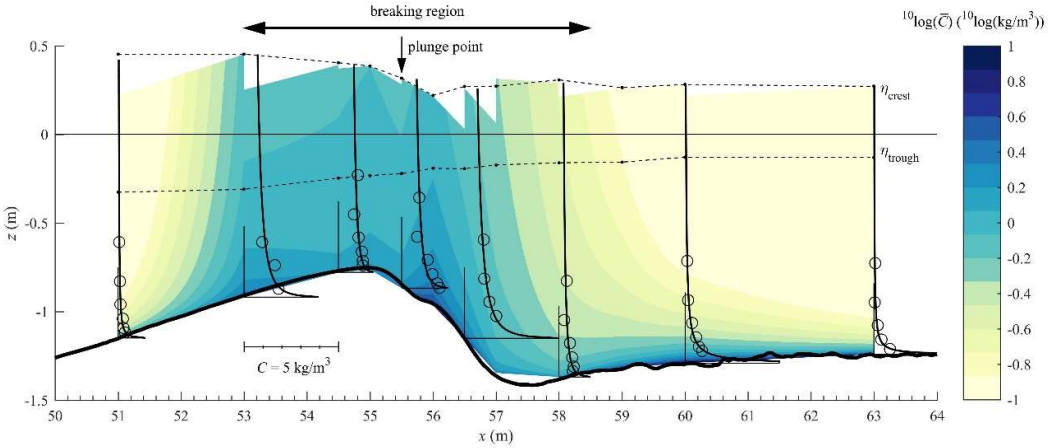

Figure 3. Time-averaged suspended sediment concentration. Open circles depict TSS measurements at eight cross-shore locations, solid curves depict fitted power function (Eq. 20). The background color contour shows the concentration field based on power-function fits at all 12 cross-shore locations.

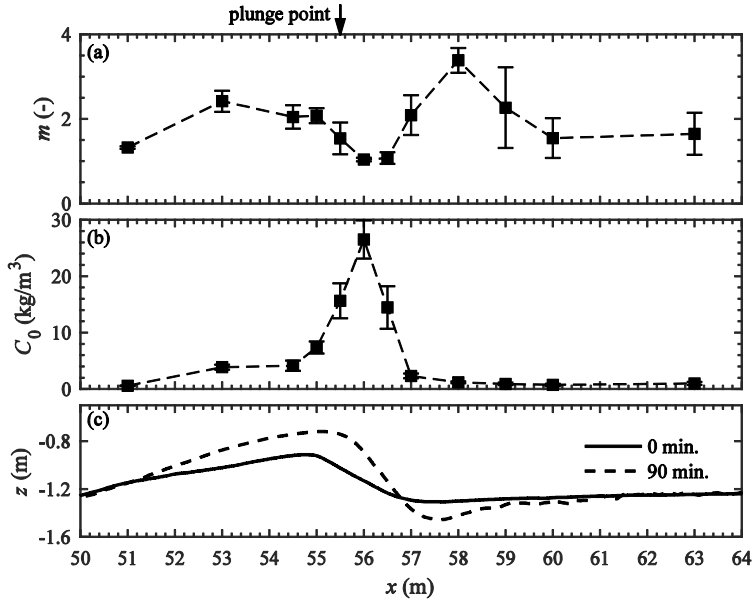

Figure 4. Cross-shore distribution of (a) vertical mixing parameter m and (b) reference concentration C_0. Values are obtained from time-averaged concentration profiles measured by ACVP over ζ = 0 to 0.10 m. Panels a-b show the means (squares) and 95% C-I (error bars) over six runs per location. (c) Bed profiles at start (solid) and end (dashed) of experiment.

3.3 Application of reference concentration model at intra-wave time scale

We now validate the adapted reference concentration model, which is given by Eq. (7) in combination with the

adapted transport parameter T_ϕ in Eq. (14), using the measurements. The model is driven using phase-averaged TKE. In the discussion (Section 4) we reflect on the time scale to which the model may be applied (i.e. instantaneous time series, phase-averaged intra-wave time scale, or wave-averaged time scale) and how this choice affects predictions of C_0.

We used the measured phase-averaged TKE $<k_b>$ inside the WBL as input for calculating T_ϕ through Eq. (14). For the present measurements, near-bed TKE profiles at the same cross-shore location showed significant run-to-run variability. This is not only due to differences in physical turbulence, but also due to uncertainties in the bed level detection. Therefore, instead of taking $<k_b>$ at one fixed elevation $\zeta = z_a$ (as per the assumptions in Section 2), we used the elevation of maximum time-averaged k_b for each run. The latter option reduced the variability in $<k_b>$ between different runs, and consequently, also led to reduced scatter in predicted C_0. The "measured" reference concentrations were extracted from the ACVP measurements as described above, i.e. the C_0 values shown in Figure 4 were used.

Figure 5 shows the measured phase-averaged velocity, measured near-bed TKE, and the modelled intra-wave C_0 for three selected cross-shore locations covering the shoaling, breaking and inner surf zone. In the shoaling zone, $<k_b>$ is continuously low as bed shear apparently generates hardly any TKE at this location (Figure 5d). In the breaking region at x = 56.0 m, i.e. the location with the strongest contribution of wave breaking turbulence to near-bed k_b, clear intra-wave time variation of $<k_b>$ is observed (Figure 5e). Highest $<k_b>$ occurs during the end of the wave trough phase, which is the main instance of wave breaking turbulence arrival at the bed for this location (vdZ16; van der A *et al.*, 2017). In the inner surf zone, where the bed is rippled, the time variation of $<k_b>$ is predominantly due to locally generated turbulence by bed friction (Figure 5f).

The intra-wave and cross-shore variation in $<k_b>$ is reflected in the modelled $<C_0>$ (Figure 5g-i). At x =51.0 m, $<k_b>$ magnitudes are so low that hardly any sand is re-suspended. In contrast, at x = 56.0 m, significant sand suspension is predicted (Figure 5h). Highest $<C_0>$ occurs during the wave trough phase, which is consistent with intra-wave vertical sand fluxes at this location (vdZ17). At x = 63.0 m, highest C_0 occurs during the wave crest phase. Measurements of time-varying near-bed concentrations support this (vdZ17).

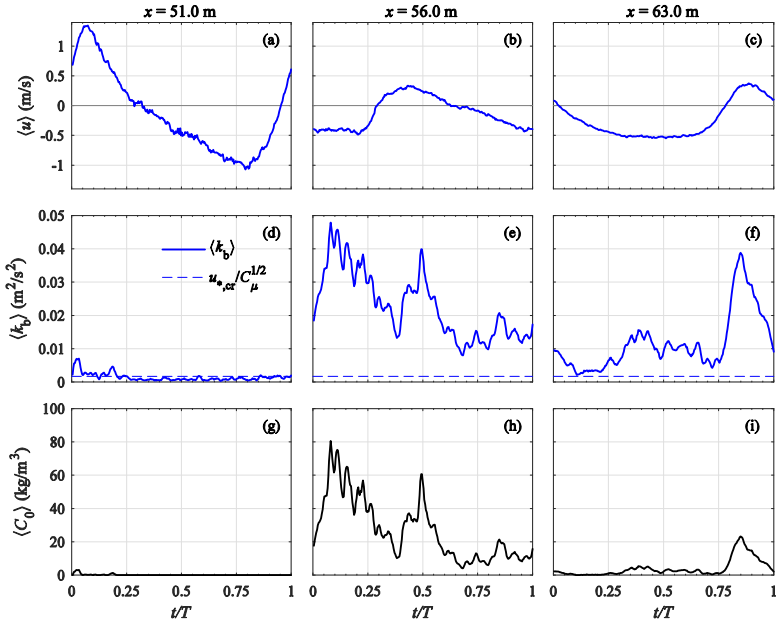

Figure 5. Application of new model (Eq. 7 and 14) to three locations: x = 51.0 m (shoaling zone, left panels); x = 56.0 m (breaking region, middle panels); x = 63.0 m (inner surf zone, right panels). (a-c) Phase-averaged horizontal free-stream velocity; (d-f) phase-averaged near-bed TKE (solid) and critical bed shear velocity over $\sqrt{C_\mu}$, i.e. threshold value for suspension (dashed); (g-i) Phase-averaged modelled reference concentration.

3.4 Evaluation of wave-averaged reference concentration

We now evaluate the model's performance at wave-averaged time scale. For comparison, C_0 was also calculated using the model by Van Rijn (2007) for combined wave and current bed shear. The phase-averaged velocities at the WBL crest-phase overshoot elevation ($\zeta \approx 0.02$ m) were used as input for Van Rijn's (2007) model.

Figure 6a shows the cross-shore distribution of C_0 obtained from the measurements and as calculated using Van Rijn's (2007) model. The model of Van Rijn (2007) predicts the correct order of magnitude for the shoaling and inner surf zone locations. However, the large increase in C_0 around the plunge point is not captured by the model. In morphodynamic models, this underestimation of C_0 would likely also result in underestimations of the suspended load and the offshore-directed suspended sand transport rate. It is further notable that Van Rijn's (2007) model overestimates C_0 in the shoaling zone at x = 51.0 m (measured C_0 = 0.6 kg/m^3; Van Rijn's model predicts 3.3 kg/m^3). At this location, sand transport occurs in a 'no suspension' sheet flow regime (c.f. Sumer *et al.*, 1996), while Van Rijn's (2007) model predicts significant suspension.

Figure 6b shows C_0 obtained using the model proposed in Section 2. The model properly predicts the cross-shore distribution of measured C_0. This is no surprise, because it was already shown that C_0 correlates well with $k_b^{3/2}$ (vdZ17). Also the order of magnitude of C_0 is generally well captured by the new model. Nevertheless, C_0 is still underestimated between x = 55.0 and 57.0 m, i.e. the region with high TKE and suspended sand loads, by about 20 to 60%. We will reflect on this in Section 4.2. Note that at x =51.0 m, the mobilisation strength of k_b does not exceed the critical bed shear velocity ($\sqrt{C_\mu}k_b < u_{*,cr}^2$), hence the model predicts no local sand resuspension. This seems consistent with the observations at this location, which showed that suspended sand was low in concentration (C_0 < 1 kg/m^3) and was formed by the smallest sand grains from the bed (D_{50} of suspended sand is approximately equal to D_{10} of sand composing the bed; see Van der Zanden, 2016). The increase in C_0 from shoaling to breaking region (x = 51.0 to 53.0 m) is properly captured by the model.

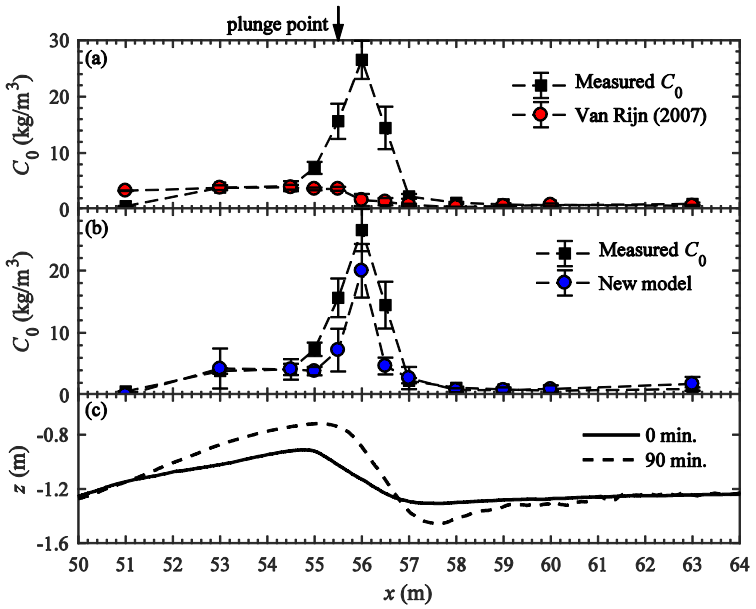

Figure 6. Cross-shore distributions of measured (square) and modelled (circles) reference concentrations. (a) Comparison with Van Rijn's (2007) model; (b) Comparison with new model, i.e. Equations (7) and (14). (c) Bed profiles at start (solid) and end (dashed) of experiment.

Both models are evaluated in more detail through Figure 7, in which measured C_0 are plotted against model predictions for all 72 runs. Due to the logarithmic scaling of the axes, the measurements at x = 51.0 m (no suspension, C_0 = 0) are not shown. The Van Rijn (2007) model shows the clustering of data points around the 1:1 line at locations offshore from the bar crest (x < 55.5 m) and in the inner surf zone ($x \geq$ 59.0 m) (Figure 7a). This suggests that for these locations, Van Rijn's model has reasonable predictive capability. However, the measured data points between bar crest and trough (55.5 $\leq x <$ 59.0 m) deviate strongly from model predictions, as Van Rijn's model does not account for wave breaking induced sand pickup. This explains the overall low r^2 of –0.25.

The new model yields an r^2 of 0.60 (Figure 7b), which is considered a reasonable-to-good correlation given the measurement uncertainties in both k_b and C_0. The figure further reveals a proper clustering of the data points around the 1:1 line for all three regions.

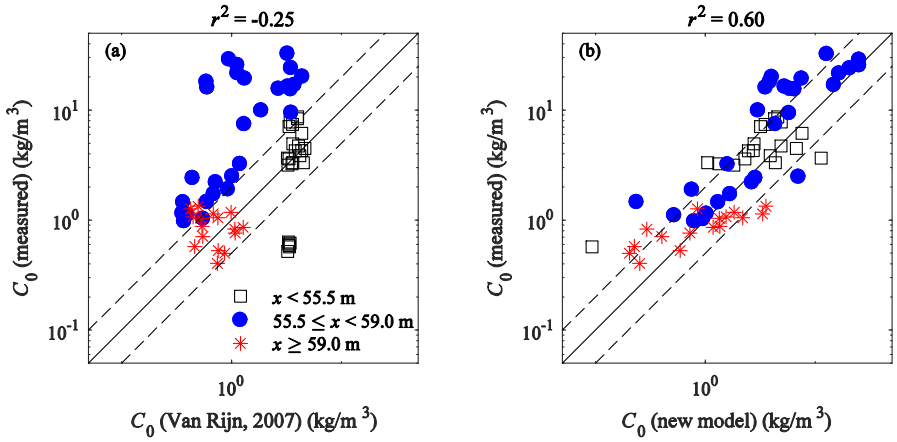

Figure 7. Scatter plots between modelled and measured C_0, using data from all 72 runs (12 cross-shore locations, six runs per location). (a) Comparison with Van Rijn's (2007) model; (b) Comparison with new model (Section 2). Solid lines mark 1:1 relation, dashed lines indicate factor 2 difference.

4. Discussion

4.1 Comparison with other approaches

The increase of pickup rates through TKE is not a novel approach for surf zone suspension. The present model shows most similarity with models of Okayasu et al. (2010) and Hsu and Liu (2004), who proposed raising the bed shear velocity by adding parameterized TKE effects. Okayasu *et al.* (2010) developed their model on the basis of steady flow measurements and is here not discussed in detail. Hsu and Liu (2004) proposed

$$u_{*,kb}^2 = u_*^2 + e_k k_{\mathrm{wbr}} \tag{21}$$

where e_k is a suspension efficiency factor due to wave breaking turbulence. Values for e_k were obtained through calibration, by simulating the small-scale experiments of Sato *et al.* (1990) with an intra-wave morphodynamic model. The pickup function was driven using numerically modelled k_{wbr} and calibrated with measured suspended sand concentrations, yielding values of e_k = 0.02 to 0.05.

Our model differs from Hsu and Liu's (2004) as we assume that k_b is the primary driver for sand suspension. At the same time our model can be rewritten into a form similar to Eq. (21), c.f. Eq. (18). It then follows that the difference between our model and Hsu and Liu's (2004) model is found in the relative sensitivity of sand suspension to k_{wbr}. We deduce that u_*^2 should be raised by $\sqrt{C_\mu} k_{\mathrm{wbr}} = 0.3 k_{\mathrm{wbr}}$, which is an order of magnitude higher than the increase by up to $0.05 k_{\mathrm{wbr}}$ as proposed by Hsu and Liu (2004). In other words, we find a much higher sensitivity of sand suspension to external TKE. For the present dataset, the factor of $0.05 k_{\mathrm{wbr}}$ by Hsu and Liu is not enough to model the increase in C_0.

Other approaches, discussed in the introduction, have proposed relating C_0 to wave parameters, such as local wave height and water depth (Mocke & Smith, 1992), wave height at the breaking point (Jayaratne & Shibayama, 2007), or the energy dissipation of the surface roller (Smith & Mocke, 1993; Spielmann et al., 2004). Although these models were not validated against the new measurements, the strong local increase in C_0 seems to correlate poorly with the aforementioned wave parameters for the present dataset. At the same time, the present dataset is unique in that it has very high spatial resolution but involves only one wave condition. The aforementioned models, in contrast, have been validated against measurements for a wider range of conditions but with more restricted spatial resolution. Hence, those models may still be a good option for capturing the general trends of increased suspended sand load from shoaling to surf zone. Nevertheless, the very local increase in C_0 should be modelled properly as the simultaneous local increase in suspended sand load and undertow velocity induces steep cross-shore gradients in cross-shore suspended sand transport rates, yielding an important contribution to breaker bar morphodynamics (c.f. vdZ17).

4.2 Time scale of model application

It should be noted that C_0 scales non-linearly to k_b, i.e. for high k_b, $C_0 \sim k_b^{3/2}$. Consequently, the time scale at which k_b is taken affects the time-averaged C_0. Highest time-averaged C_0 is expected when a time series of instantaneous $k_b(t)$ is used to force the model: the distribution of k_b is positively skewed, and events of high $k_b(t)$ will result in strong resuspension events that contribute greatly to time-averaged C_0. If, instead, wave-averaged $\overline{k}_b$ is used to

force the model, time-averaged C_0 will be significantly lower. The new reference concentration model was here applied at an intra-wave time scale, using phase-averaged $<k_b>$ as input. If the model is forced with wave-averaged $\overline{k_b}$, modelled C_0 values decrease by 15% and the agreement between model and data reduces slightly (r^2 decreases from 0.60 to 0.57). For the present dataset, the model could not be applied to a time series of $k_b(t)$ because these time series were for some locations contaminated with acoustic noise that could only be removed during the ensemble-averaging procedure (see vdZ16).

Depending on the type of morphodynamic model used, the new reference concentration approach based on k_b may be used to simulate the instantaneous intermittent sand suspension (Scott et al., 2009), the intra-wave phase-dependent suspension due to intra-wave k_b behaviour (Brinkkemper et al., 2017; vdZ17), or the increased reference concentrations at wave-averaged time scale (Aagaard & Jensen, 2013; Nielsen, 1984) under breaking waves.

4.3 Applicability in morphodynamic models

The proposed reference concentration model only requires near-bed TKE as input, hence its implementation is straightforward. However, a proper performance of the model relies greatly on the accuracy of the modelled k_b. The quantification of both the bed-generated and the breaking-generated TKE contributions is a challenge for turbulence models (Justesen *et al.*, 1987). Fernández-Mora *et al.* (Submitted) showed that even with high temporal (intra-wave) and spatial (1 mm vertical grid height to resolve the WBL) resolution, state-of-the-art CFD models have major difficulties predicting the spatial trends and magnitudes of near-bed TKE. It should also be mentioned that k_b is strongly non-uniform across the breaking region and the breaker bar, and a high cross-shore resolution (Δx << local wave length L) is required for modeling the very local increase in k_b and C_0.

Another issue is that many morphodynamic models do not resolve the WBL flow, and use a bottom boundary condition for k_b based purely on local bed shear stress, i.e. $k_b = u_*^2/\sqrt{C_\mu}$ (Eq. 11). With this boundary condition, the propagation of breaking-generated TKE into the WBL can only be simulated when the WBL flow is accurately resolved. An alternative approach for simulating the wave breaking TKE arrival at the bed is to adopt a higher-order bottom boundary condition for k_b (as also argued by Hsu & Liu, 2004).

Another method to overcome the challenge of numerically predicting k_b is the use of idealised formulations where k_b is related to breaking wave conditions (c.f. Roelvink & Stive, 1989; Steetzel, 1993). However, although the formulation by Roelvink and Stive (1989) has gained popularity especially for application in depth-averaged morphodynamic models (Reniers *et al.*, 2013; Reniers *et al.*, 2004; Van Thiel de Vries, 2009), to the authors' knowledge it has never been validated against accurate measurements of k_b under breaking waves.

5. Conclusion

Based on theoretical considerations and using widely applied formulations, we derived a new formulation for reference concentrations and pickup rates for surf zone conditions that does not involve further empirical calibration parameters. The model is based on Van Rijn's (1984c) reference concentration model and assumes wave breaking TKE as driving parameter for sand re-suspension. The new model was validated using a new dataset of collocated near-bed turbulent kinetic energy and suspended sand concentration (van der Zanden *et al.*, 2016; 2017). The model shows good agreement between modelled and measured reference concentration ($r^2 = 0.60$).

The new reference concentration model can be applied in morphodynamic models operating at intra-wave or wave-averaged time scales. However, one needs to be aware that the proposed reference concentration model requires accurate predictions of the combined bed-generated and wave breaking produced turbulent kinetic energy at close distance from the bed.

Acknowledgments

The research presented in this paper is conducted within the SINBAD project, funded by STW (12058) and EPSRC (EP/J00507X/1, EP/J005541/1), and received additional funding through Hydralab IV (European Community FP7, contract no. 261520) and Hydralab+ (EC Horizon 2020 programme, contract no. 654110). The authors thank Minfei He (University of Twente) and Peng Zheng (University of Liverpool) for insightful discussions on this topic.

References

Aagaard, T., & Jensen, S. G. (2013). Sediment concentration and vertical mixing under breaking waves. *Marine Geology, 336*, 146-159.
Brinkkemper, J. A., de Bakker, A. T. M., & Ruessink, B. G. (2017). Intrawave sand suspension in the shoaling and surf zone of a field-scale laboratory beach. *Journal of Geophysical Research: Earth Surface*.
Cox, D. T., & Kobayashi, N. (2000). Identification of intense, intermittent coherent motions under shoaling and breaking waves. *Journal of Geophysical Research-Oceans, 105*(C6), 14223-14236.
Cox, D. T., Kobayashi, N., & Okayasu, A. (1996). Bottom shear stress in the surf zone. *Journal of Geophysical Research-Oceans, 101*(C6), 14337-14348.
Fernández-Mora, A., Ribberink, J. S., Van der Zanden, J., van der Werf, J. J., & Jacobsen, N. G. (Submitted). RANS-VOF modeling of full-scale wave breaking processes. *Ocean Dynamics*, manuscript in review
Hinze, J. O. (1975). *Turbulence*. New York: McGraw-Hill.
Hsu, T. J., & Liu, P. L. F. (2004). Toward modeling turbulent suspension of sand in the nearshore. *Journal of Geophysical Research-Oceans, 109*(C6).
Hurther, D., Thorne, P. D., Bricault, M., Lemmin, U., & Barnoud, J. M. (2011). A multi-frequency Acoustic Concentration and Velocity Profiler (ACVP) for boundary layer measurements of fine-scale flow and sediment transport processes. *Coastal Engineering, 58*(7), 594-605.
Jayaratne, R. M. P., & Shibayama, T. (2007). Suspended Sediment Concentration on Beaches under Three Different Mechanisms. *Coastal Engineering Journal, 49*(04), 357-392.
Justesen, P., Fredsøe, J., & Deigaard, R. (1987). *The Bottleneck Problem for Turbulence in Relation to Suspended Sediment in the Surf Zone*. Proc. 20th Inernational Conference on Coastal Engineering, Taipei, Taiwan
Kobayashi, N., & Johnson, B. D. (2001). Sand suspension, storage, advection, and settling in surf and swash zones. *Journal of Geophysical Research, 106*(C5), 9363-9376.
Kranenburg, W. M., Ribberink, J. S., Uittenbogaard, R. E., & Hulscher, S. J. M. H. (2012). Net currents in the wave bottom boundary layer: On waveshape streaming and progressive wave streaming. *Journal of Geophysical Research F: Earth Surface, 117*(3).
Mocke, G. P., & Smith, G. G. (1992). *Wave breaker turbulence as a mechanism for sediment suspension*. Proc. 23rd International Conference on Coastal Engineering, Venice, Italy.
Nadaoka, K., Ueno, S., & Igarashi, T. (1988). Sediment suspension due to large scale eddies in the surf zone. *Proceedings of the 21st International Conference on Coastal Engineering, Torremolimos, Spain*, 1646-1660.
Nielsen, P. (1984). Field-Measurements of Time-Averaged Suspended Sediment Concentrations under Waves. *Coastal Engineering, 8*(1), 51-72.
Nielsen, P. (1986). Suspended Sediment Concentrations under Waves. *Coastal Engineering, 10*(1), 23-31.
Nielsen, P. (1992). *Coastal Bottom Boundary Layers and Sediment Transport* (Vol. 4). Singapore: World Scientific.
Okayasu, A., Fujii, K., & Isobe, M. (2010). *Effect of external turbulence on sediment pickup rate*. Proc. 32nd International Conference on Coastal Engineering.
Pope, S. B. (2000). *Turbulent Flows*: Cambridge University Press.
Reniers, A. J. H. M., Roelvink, J. A., & Thornton, E. B. (2004). Morphodynamic modeling of an embayed beach under wave group forcing. *Journal of Geophysical Research-Oceans, 109*(C1). doi:10.1029/2002jc001586
Reniers, A. J. H. M., Gallagher, E. L., MacMahan, J. H., Brown, J. A., van Rooijen, A. A., de Vries, J. S. M. V., & van Prooijen, B. C. (2013). Observations and modeling of steep-beach grain-size variability. *Journal of Geophysical Research-Oceans, 118*(2), 577-591.
Ribberink, J. S., Van der A, D. A., Van der Zanden, J., O'Donoghue, T., Hurther, D., Cáceres, I., & Thorne, P. D. (2014). *SandT-Pro: Sediment transport measurements under irregular and breaking waves*. Proc. of the 34th International Conference on Coastal Engineering, Seoul, Korea
Roelvink, J. A., & Stive, M. J. F. (1989). Bar-Generating Cross-Shore Flow Mechanisms on a Beach. *Journal of Geophysical Research-Oceans, 94*(C4), 4785-4800.
Ruessink, B. G., van den Berg, T. J. J., & van Rijn, L. C. (2009). Modeling sediment transport beneath skewed asymmetric waves above a plane bed. *Journal of Geophysical Research, 114*(C11).
Sato, S., K. Homma, & Shibayama, T. (1990). Laboratory study on sand suspension due to breaking waves. *Coastal Engineering Japan*, 33, 219– 231
Scott, N. V., Hsu, T. J., & Cox, D. (2009). Steep wave, turbulence, and sediment concentration statistics beneath a breaking wave field and their implications for sediment transport. *Continental Shelf Research, 29*(20), 2303-2317.
Smith, G. G., & Mocke, G. P. (1993). *Sediment suspension by turbulence in the surf zone*. Proc. Euromech 1993, Le Havre, France.
Spielmann, K., Astruc, D., & Thual, O. (2004). Analysis of some key parametrizations in a beach profile morphodynamical model. *Coastal Engineering, 51*(10), 1021-1049.
Steetzel, H. (1993). *Cross-shore transport during storm surges.* PhD thesis, Delft University of Technology.
Sumer, B. M., Chua, L. H. C., Cheng, N. S., & Fredsoe, J. (2003). Influence of turbulence on bed load sediment transport. *Journal of Hydraulic Engineering-Asce, 129*(8), 585-596.
Sumer, B. M., Kozakiewicz, A., Fredsoe, J., & Deigaard, R. (1996). Velocity and Concentration Profiles in Sheet-Flow Layer of Movable Bed. *Journal of Hydraulic Engineering, 122*(10), 549-558.
Sumer, B. M., Guner, H. A. A., Hansen, N. M., Fuhrman, D. R., & Fredsøe, J. (2013). Laboratory observations of flow and sediment transport induced by plunging regular waves. *Journal of Geophysical Research: Oceans, 118*(11), 6161-6182.
Svendsen, I. A., Madsen, P. A., & Buhr Hansen, J. (1978). *Wave characteristics in the surf zone*. Proc. 16th Conf. Coastal Eng., Hamburg, Germany.

Svendsen, I. A. (1987). Analysis of Surf Zone Turbulence. *Journal of Geophysical Research-Oceans, 92*(C5), 5115-5124.
Ting, F. C. K., & Kirby, J. T. (1995). Dynamics of Surf-Zone Turbulence in a Strong Plunging Breaker. *Coastal Engineering, 24*(3-4), 177-204.
Van der A, D. A., Van der Zanden, J., O'Donoghue, T., Hurther, D., Cáceres, I., McLelland, S. J., & Ribberink, J. S. (2017). Large-scale laboratory study of breaking wave hydrodynamics over a fixed bar. *Journal of Geophysical Research: Oceans*, in press.
Van der Zanden, J., Alsina, J. M., Cáceres, I., Buijsrogge, R. H., & Ribberink, J. S. (2015). Bed level motions and sheet flow processes in the swash zone: Observations with a new conductivity-based concentration measuring technique (CCM+). *Coastal Engineering, 105*, 47-65.
Van der Zanden, J., van der A, D. A., Hurther, D., Cáceres, I., O'Donoghue, T., & Ribberink, J. S. (2016). Near-bed hydrodynamics and turbulence below a large-scale plunging breaking wave over a mobile barred bed profile. *Journal of Geophysical Research: Oceans, 121*(8), 6482-6506.
Van der Zanden, J., Van der A, D. A., Hurther, D., Caceres, I., O'Donoghue, T., & Ribberink, J. S. (2017). Suspended sediment transport around a large-scale laboratory breaker bar. *Coastal Engineering, in press*.
Van der Zanden, J., Van der A, D. A., Hurther, D., Caceres, I., O'Donoghue, T., Hulscher, S. J. M. H., & Ribberink, J. S. (Submitted). Bedload and suspended load contributions to the morphodynamics of a large-scale laboratory breaker bar. *Coastal Engineering*.
Van der Zanden, J. (2016). *Sand Transport Processes in the Surf and Swash Zones.* PhD Thesis, University of Twente, the Netherlands.
Van Rijn, L. C. (1984a). Sediment Pick-Up Functions. *Journal of Hydraulic Engineering, 110*(10), 1494-1502.
Van Rijn, L. C. (1984b). Sediment Transport, Part I: Bed Load Transport. *Journal of Hydraulic Engineering, 110*(10), 1431-1456.
Van Rijn, L. C. (1984c). Sediment Transport, Part II: Suspended Load Transport. *Journal of Hydraulic Engineering, 110*(11), 1613-1641.
Van Rijn, L. C. (2007). Unified View of Sediment Transport by Currents and Waves. II: Suspended Transport. *Journal of Hydraulic Engineering, 133*(6), 668-689.
Van Thiel de Vries, J. S. M. (2009). *Dune erosion during storm surges.* PhD Thesis, TU Delft, Delft.
Yoon, H. D., & Cox, D. T. (2012). Cross-shore variation of intermittent sediment suspension and turbulence induced by depth-limited wave breaking. *Continental Shelf Research, 47*, 93-106.
Zhou, Z., Hsu, T.-J., Cox, D., & Liu, X. (2017). Large-eddy simulation of wave-breaking induced turbulent coherent structures and suspended sediment transport on a barred beach. *Journal of Geophysical Research: Oceans*.
Zyserman, J. A., & Fredsøe, J. (1994). Data Analysis of Bed Concentration of Suspended Sediment. *Journal of Hydraulic Engineering, 120*(9), 1021-1042.